International Journal of Economy, Energy and Environment
2019; 4(2): 24-32
http://www.sciencepublishinggroup.com/j/ijeee
doi: 10.11648/j.ijeee.20190402.11
ISSN: 2575-5013 (Print); ISSN: 2575-5021 (Online)

Effects of the Ba Impregnation on Pt Electrode on NO Electrochemical Reduction Mechanism

Xi Wang

Jiangsu Investment Management Co., Ltd., Nanjing, China

Email address:
175574373@qq.com

To cite this article:
Xi Wang. Effects of the Ba Impregnation on Pt Electrode on No Electrochemical Reduction Mechanism. *International Journal of Economy, Energy and Environment*. Vol. 4, No. 2, 2019, pp. 24-32. doi: 10.11648/j.ijeee.20190402.11

Received: June 5, 2019; **Accepted**: July 16, 2019; **Published**: July 19, 2019

Abstract: The study investigated the electrochemical reduction performances of NO and O_2 on Pt symmetric electrode with Ba adsorption layer. The temperature varied from 350°C to 550°C. The experimental Ba $(NO_{3)2}$ solution was impregnated in the Pt electrode. For the NO performance, the polarization curves and CV tests showed that the Pt-BaO electrode showed higher electrochemical performance than Pt electrode. EIS results revealed that the Pt-BaO electrode exhibited higher activity than the Pt electrode. It was due to the decreased polarization resistance in the low-frequency region that dominated the electrochemical impedance spectra. The increase of temperature strengthened the effect of adsorption layer on NO electrochemical performance. The EIS results were fitted well with the equivalent circuit model indicating that the improved mechanism with the Ba adsorption layer may be related with the NO oxidation to NO_2 on the Pt surface, the formation of Ba $(NO_3)_2$ in the adsorption layer and the reduction of the reaction path from the direct Ba $(NO_3)_2$ decomposition.

Keywords: Symmetric Electrode, Electrochemical Performance, Electrochemical Impedance Spectra, Equivalent Circuit Model

1. Introduction

Nitrogen oxides are the main exhaust pollutants emitted by diesel engines and gasoline engines. These pollutants (mainly NO) are discharged directly into the environment without purification can have a huge impact on the environment [1-3]. It can cause acid rain, photochemical smog. Traditional removal technology of nitrogen oxides is selective catalytic reduction (SCR) technology. The excess of O_2 in these pollutants causes the removal of nitrogen oxides incompletely [4-6]. Electrochemical removal of NO by using solid oxide electrolysis cell (SOEC) avoids the produced pollutions such as CO, CH_x. Besides, it saves the large reducing agents storage system [7-12].

In the electrolysis cathode, NO can be reduced to N_2 and O^{2-}. O^{2-} can be transferred to anode and oxidized to O_2 under external electric field. Electrochemical reduction of NO can be operated at low temperature range that fits well with the exhausts temperature from the diesel/gasoline engine. Nevertheless, it confronted with the difficulties of NO selectivity improvement and conversion performance in the excess O_2 exhausts. An efficient method that has been carried out in previous studies [13-16] is by adding NOx adsorption layer on the electrode to constitute a multi-functional electrode layer. The adsorption layer is also named three-way catalyst (TWC). In this way, NOx can be trapped and stored in the adsorption layer. The NOx selectivity and activity can be strengthened.

Bredikin [17-19] et al studied NO electrochemical performance on the Pt electrode coated with NiO/YSZ composite layer. Results showed that NO conversion can be improved due to the formed nanometer microstructure in the NiO/YSZ layer by increasing the reactive cites. The proposed reaction mechanism was that the reduced Ni metal played the role of transferring oxygen species in the reaction processes. Hamamoto [20] investigated three different NOx adsorption layers of $Na/Pt/Al_2O_3$, $Cs/Pt/Al_2O_3$, $K/Pt/Al_2O_3$ on NO conversion performances. From the results, it can be concluded that $K/Pt/Al_2O_3$ exhibited the best performance and the NO conversion reached 80%. The NO conversion was only 60% in the blank Pt electrode without the adsorption layers. Vernoux [21] impregnated BaO on the Pt electrode and studied the NOx storage-reduction (NSR)

process in the Pt-BaO/YSZ cell at 350°C and 400°C. It can be obtained from the results that the NOx storage-reduction process can be characterized in situ. It can be due to the variations of the catalyst potential. Later, he [22] observed electrochemical promotion of catalysis (EPOC) effect on an electrochemically-assisted NSR catalyst electrodes containing Ba adsorption layer. It was proposed by Vayenas [23]. The principle was that the promoter ions such as O^{2-}, K^{+} can be produced. These promoter ions can be electrochemically supplied to the catalyst surface by applying polarization between the catalyst electrode and the counter electrode. The catalytic performance can be changed by the modification of the catalyst work function. Conclusions were made that Ba containing catalyst showed better activity than Ba free electrode. An electromotive force(EMF) was formed between the nanometer Pt and Rh electrodes. This EMF induced the self-sustained electrochemical promotion effect that in turn enhanced the catalytic activity. The promotion effect was named as Non-Faraday Electrochemical Modification of Catalytic Activity Effect(NEMCA) [24].

Traulsen et al [25] added KNO_3 and MnOx adsorption layer in the LSM/GDC electrode. Cyclic voltammetry (CV) and electrochemical impedance spectroscope (EIS) experiment results demonstrated that KNO_3 can be used for NOx storage but MnOx. Both the impregnation of KNO_3 and MnOx can cause the decrease of the polarization resistance related to the formation of NO_2 from NO oxidation. They [26-27] also applied K_2O, BaO on the $La_{0.85}Sr_{0.15}FeO_3/Ce_{0.9}Gd_{0.1}O_{1.95}$ (LSF-GDC) and $La_{0.85}Sr_{0.15}MnO_3/Ce_{0.9}Gd_{0.1}O_{1.95}$ (LSM-GDC) composite electrodes respectively based on the GDC electrolyte cell stacks. Results showed that high NOx conversion can be obtained with the NOx adsorption layer between 300°C and 500°C. Shao [28] later investigated NO electrochemical reduction characteristics on LSM-GDC electrode containing $Ba/Pt/Al_2O_3$ adsorption layer in the direct current (DC) and square wave (SV) electrolysis. The NOx trapping and reduction rates can be balanced in the SV electrolysis indicating the further improvement. She [29] further demonstrated that the improvement mechanism was to promote the adsorption and surface diffusion of NOx species near/at the triple phase boundary (TPB) and the $K/Pt/Al_2O_3$ layer showed better performance than the $Ba/Pt/Al_2O_3$ layer toward NO reduction. According to the above studies, the further reaction mechanism for NO electrochemical reduction in the adsorption layer was not clear. And the electrochemical performance of NO reduction required further investigation to illustrate the interior reaction mechanism.

This paper investigated the electrochemical reduction of NO and O_2 on symmetric Pt electrode by adding Ba NOx adsorbents. Two cells were prepared and tested: single Pt electrode, Pt electrode with Ba $(NO_3)_2$ impregnation (Pt-BaO electrode). Linear sweep voltammetry, cyclic voltammetry (CV) and EIS measurements were carried out between 350°C and 550°C. Detailed reaction processes were characterized by EIS fitted results in different frequency range.

2. Experiment Tests

2.1. Cell Preparation

Two symmetric cells Pt/YSZ/Pt were prepared coating with Pt electrode by screen printing method and sintered at 900°C for 1h in air. And the Pt electrode area was 3.14cm^2. YSZ was used as the electrolyte. One cell was impregnated with Ba $(NO_3)_2$ solution for 1 min by the suction filtration of the pump. The concentration of the Ba $(NO_3)_2$ was 0.32mol/L. The Ba impregnation cell was sintered at 700°C for 1 h after it was dried in air.

2.2. Experiment Measurements

The electrochemical experiments were tested by ZAHNER (Germany) from 350°C to 550°C. The EIS tests were recorded in the frequency range of 100kHz to 0.1Hz with the amplitude of 10 mV. For the linear sweep voltammetry measurements, the voltage was set from 2V to 0V at the scanning rate of 20mV/s. And CV tests scanned from 0.5V to -0.5V at the rate of 10mV/s. The inlet gases were composed of 800ppm NO, 8% O_2 and Ar was used as the carrier gas. The total flow rate was set at 100ml/min. All the gas concentrations were chosen according to the engine exhausts. The EIS measurements fitted with the equivalent circuit model (ECM) were analyzed by the ZsimpWin software. The EIS results analyzed by the equivalent circuit model proved to be important for the understanding of the strengthened selectivity mechanism of NO. This analyzing method was adopted by Shao [30] in the thesis.

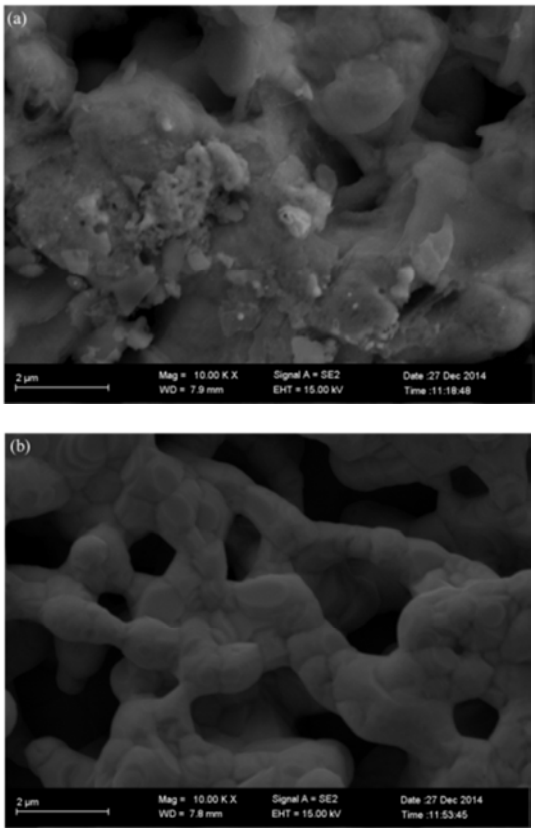

Figure 1. *Surface microstructure images for the two electrodes: (a) Ba impregnated electrode (b) Non-impregnated Pt electrode.*

Both of the two types of the cell microstructure were characterized by scanning electron microscope (SEM) after testing. It can be shown from the figure 1 (a) that the SEM image of the Ba impregnated cell presented small and distinct BaO particles over the Pt electrode surface according to the energy dispersive spectrometer (EDS) results. The blank Pt electrode presented regular porous microstructure.

3. Results and Discussion

3.1. Current Voltage (I-V) Characteristics

Figure 2 gives the polarization curves of the NO electrochemical reduction on Pt electrode and Pt-BaO electrode at 440°C and 550°C. The tests were conducted in 800ppm NO. Ar was the carrier gas. At higher temperatures and voltages (1.25V to 2V), it could be observed that the Ba impregnated electrode exhibited higher electrochemical performance than the blank Pt electrode. It was explained that NO can be stored in the Ba active sites in the adsorption layer in the form of Ba $(NO_3)_2$. Thus, the reaction kinetics on the Pt-BaO surface was strengthened. And the electrochemical reaction processes can be accelerated by the reduction of reaction path. Here refered to the Ba $(NO_3)_2$ decomposition to N_2 directly with external electrical field. The reaction phenomenon was similar discovered by Shao [28-29] in the experiments.

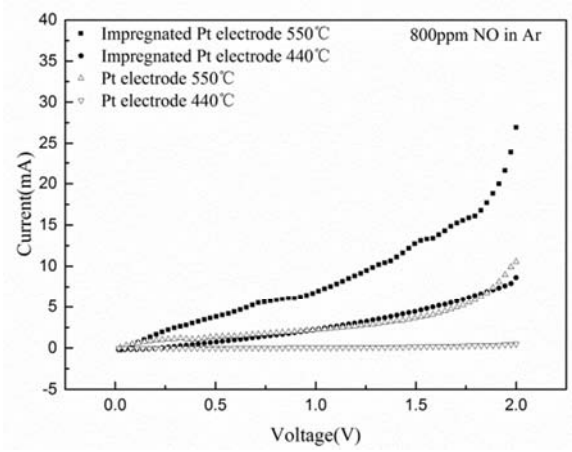

Figure 2. *Polarization curves of 800ppm NO in Ar on Pt-Ba electrode and Pt electrode at 550°C and 440°C.*

3.2. Cyclic Voltage Measurements

Figure 3 to 6 show the electrochemical performances of the Pt electrode and Pt-BaO electrode in 8%O_2, 800ppmNO atmospheres by cyclic voltammetry with the temperature varying from 350°C to 450°C. The sweep rate was set at 10mV/s. As shown in figure 3 and 4, the Pt electrode showed better activity and selectivity in O_2 atmosphere than in pure NO atmosphere at 440°C. A small hysteresis was observed in both two atmospheres. When changed the sweep direction from negative voltage to anodic voltage, the reduction peaks of NO and O_2 were observed. And the NO reduction peak appeared earlier than O_2. The increase of the current with temperature in O_2 atmosphere was more significant than that in pure NO atmosphere.

It can be obtained from figure 5 and 6 that Pt-BaO electrode was superior to the blank Pt electrode in 800ppm NO atmosphere due to the storage of NO in the adsorption layer. The effect of the Ba adsorption layer became more significant as the temperature increased to 440°C. It can be concluded that the increase of activity with temperature on the Pt-BaO electrode was more obviously in NO atmosphere compared with the Pt electrode.

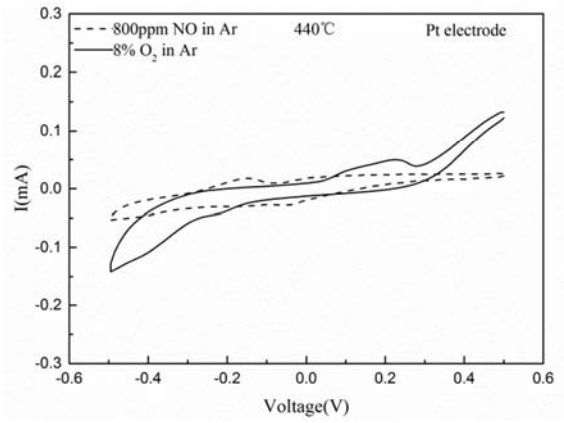

Figure 3. *Cyclic voltammograms on Pt electrode in different atmospheres at 440°C.*

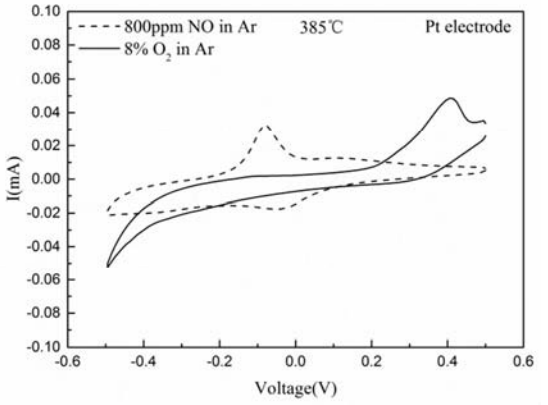

Figure 4. *Cyclic voltammograms on Pt electrode in different atmospheres at 385°C.*

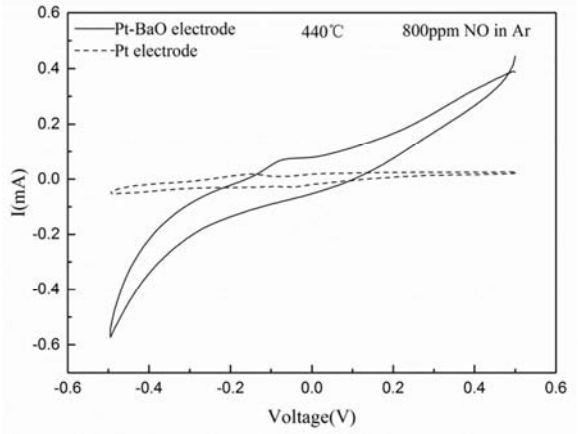

Figure 5. *Cyclic voltammograms of 800ppm NO in Ar on Pt-BaO electrode and Pt electrode at 440°C.*

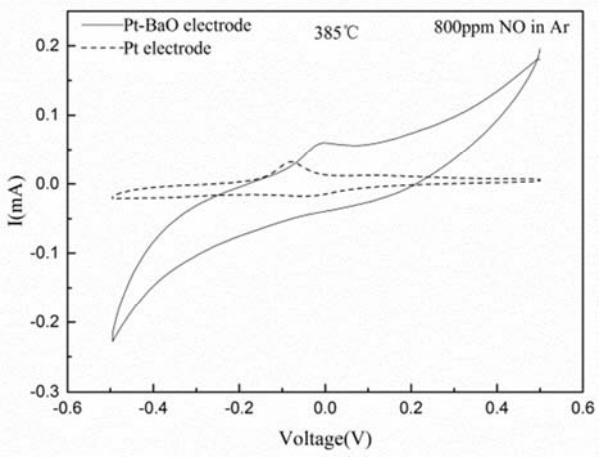

Figure 6. *Cyclic voltammograms of 800ppm NO in Ar on Pt-BaO electrode and Pt electrode at 385°C.*

3.3. EIS Results

The EIS measurements in different atmospheres were conducted on the two types of the cells from 350°C to 550°C at open circuit voltage (OCV) that were shown from figure 7 to figure 10. Three different gas atmospheres were investigated: 800ppm NO with 8% O_2, 800ppm NO and 8% O_2. Ar was used as the carrier gas. It can be seen from figure 7 to figure 10 that the Pt-BaO electrode presented lower resistance than the Pt electrode in three atmospheres with the temperature ranging from 350°C to 550°C. At high temperature of 550°C and 440°C, the resistance in O_2 appeared larger than in NO with O_2 mixtures on two cells which was close to the results conducted by Shao [29]. This may be due to the formation of NO_2 from NO oxidation with O_2 on Pt electrode surface. As temperature decreased, the impedance spectra in O_2 atmosphere showed the largest. And the spectra in three atmospheres became close to each other on two cells. The resistance in NO with O_2 atmosphere showed the lowest in Pt-BaO electrode which was related to the NO_2 formation from NO oxidation process that decreased the activation energy. The formation of Ba $(NO_3)_2$ from NO or NO_2 accelerated the reaction rates. The Warburg diffusion process was observed in low frequency region. The phenomenon became obvious at lower temperature. This was related to the increased diffusion resistance at lower temperatures.

As shown in figure 8 to 10, the decrease of temperature increased the resistances in three atmospheres on both two cells. And the observation was similar to the phenomenon in figure 7. The impedance spectra in NO with O_2 showed similar characteristics compared with pure O_2 atmosphere on two cells. To be different, the resistances in three atmospheres on Pt-BaO electrode were close to each other with the decrease of the temperature. The resistances in O_2 atmosphere exhibited the largest on two electrodes. And the resistance in NO and O_2 mixtures exhibited smaller compared with the resistance in O_2 atmosphere. In a word, the electrochemical performance on Pt-BaO electrode was superior to that on Pt electrode. The storage of NOx in the form of Ba $(NO_3)_2$ in active sites or the direct electrolysis of Ba $(NO_3)_2$ in external electric field can enhance the reactivity and selectivity of NO reduction performances.

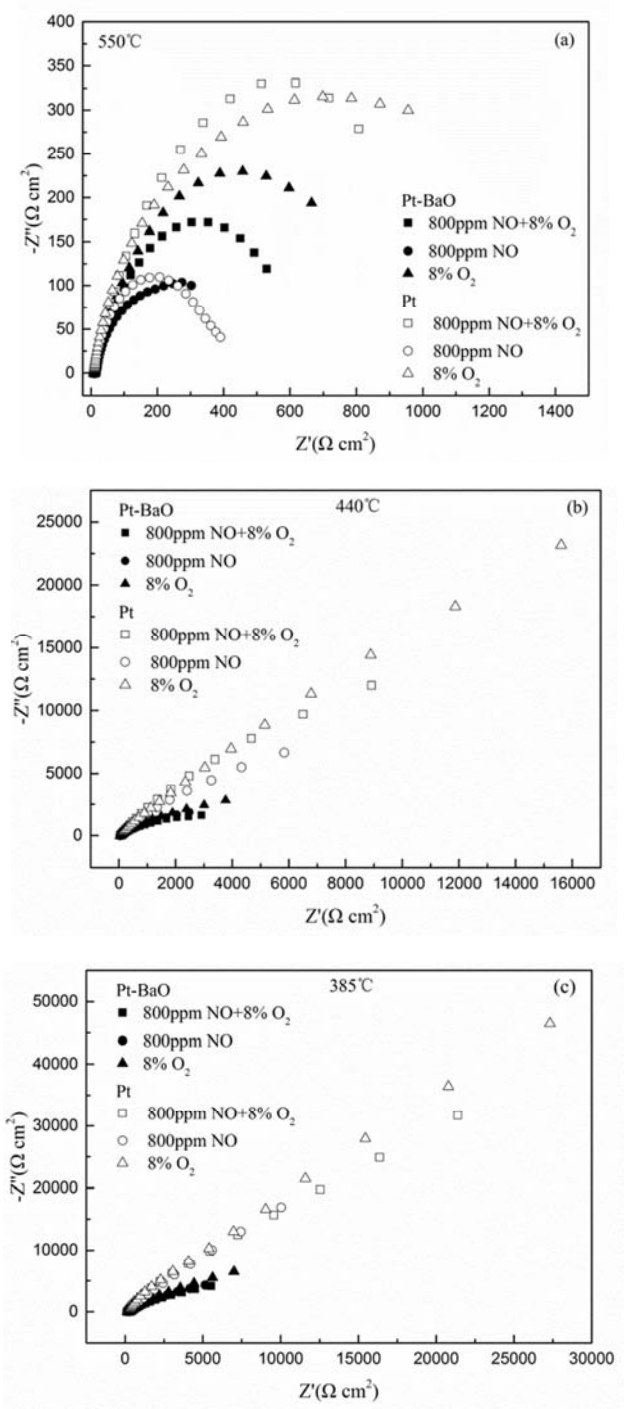

Figure 7. *EIS for Pt-BaO electrode and Pt electrode in different atmospheres from 350°C to 550°C: (a)550°C; (b)440°C; (c)385°C.*

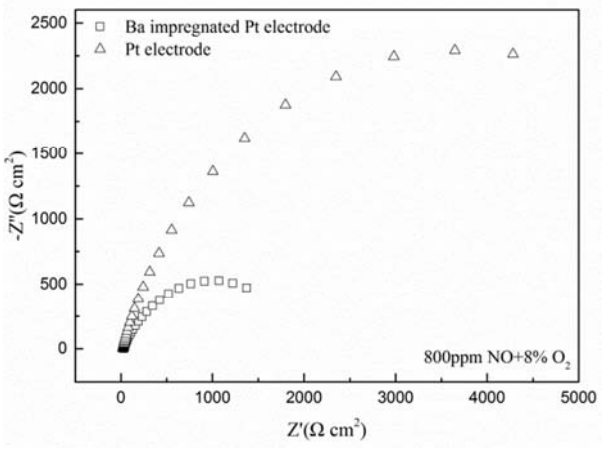

Figure 8. *EIS for Pt-BaO electrode and Pt electrode in 800ppm NO with 8% O_2 at 495°C.*

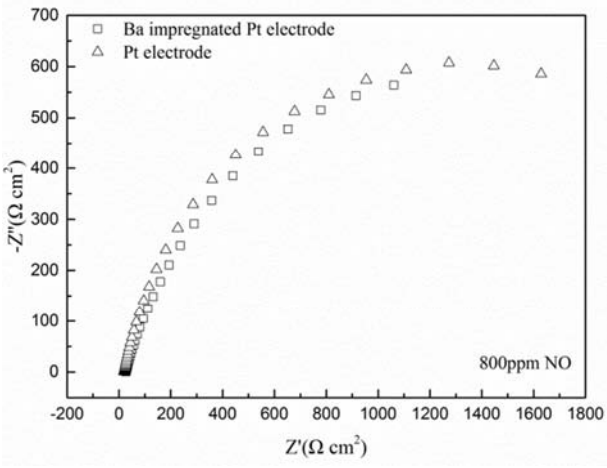

Figure 9. *EIS for Pt-BaO electrode and Pt electrode in 800ppm NO at 495°C.*

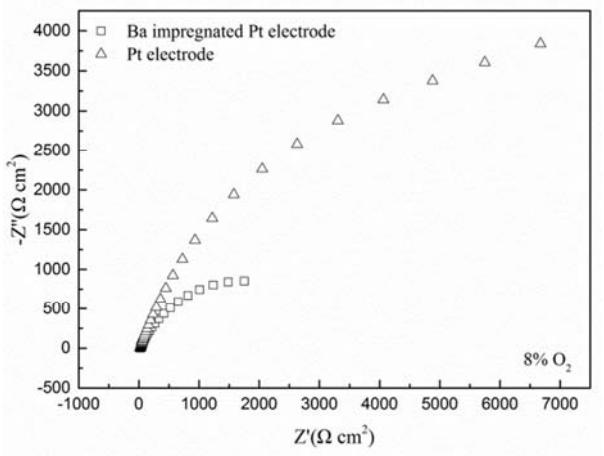

Figure 10. *EIS for Pt-BaO electrode and Pt electrode in 8% O_2 at 495°C.*

3.4. EIS Results Fitting to the Equivalent Circuit Model

An equivalent circuit model contained electrolyte serial resistance Rs (relative to the conductivity of the electrolyte), serial RC elements were used for fitting the impedance spectra by experiments. A polarization resistance is in parallel with a capacitance C. In the nonlinear system, the capacitance can be substituted as the constant phase element (CPE). Shao [30] also adopted this similar model for analyzing the reaction mechanism of the NO electrochemical reaction. The constituent elements of the model were different according to different reaction processes that occurred. It varied from each other according to the experiment results conducted by different researchers.

The schematic of the equivalent circuit model can be showed in figure 11: one serial resistance Rs and 3 RC elements.

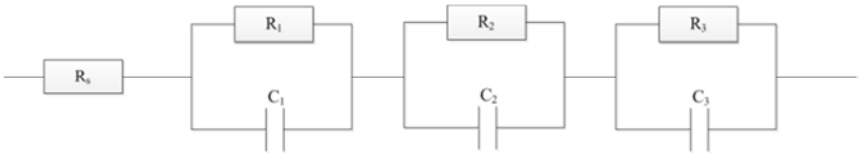

Figure 11. *Schematic of the equivalent circuit model.*

The impedance for the constant phase element can be written as follows:

$$Z=\frac{1}{jwY_0} \tag{1}$$

Y_0 is the admittance of the impedance. The equivalent capacitance of the capacitance element (C) can be expressed as C_w :

$$C_w = Y_0 \tag{2}$$

The summit frequency of the semicircle can be expressed as follows:

$$f_m = \frac{1}{2\pi RC_w} \tag{3}$$

The activation energy E of the reaction processes can be calculated as follows:

$$\delta = \delta_0 \exp(-\frac{E}{k_B T}) \tag{4}$$

δ represents the electrical conductivity and δ_0 is the pre-exponential factor. k_B (1.38×10^{-23} J/K) is the Boltzmann constant. T is the absolute temperature (K).

The characteristics of the impedance spectra from the fitted results in three different atmospheres from 350°C to 550°C were listed in Table 1 to 6 on two cells. The polarization resistances were composed of R_1, R_2 and R_3. C_w was the value of the capacitance element. As temperature decreased, the capacitance in three arcs decreased especially in arc 1. The capacitances in three different arcs at the same temperature were close to each other.

Table 1. *ECM results of Pt electrode in 800ppm NO and 8% O_2.*

T (°C)	R_s (Ω m^2)	R_n(Ω m^2)			C_w(×10^{-4} F cm^{-2})		
		R_1	R_2	R_3	C_1	C_2	C_3
550	9.541	12.77	121.5	694.7	0.98	2.273	5.907
495	22.14	28.87	558.9	4560	0.5127	0.7521	1.341
440	62.93	63.63	1133	2.331×10^4	0.2134	0.492	0.7341
385	167.4	95.79	3955	6.318×10^4	0.05818	0.1645	0.2982

Table 2. *ECM results of Pt electrode in 800ppm NO.*

T (°C)	R_s (Ω m^2)	R_n(Ω m^2)			C_w(×10^{-4} F cm^{-2})		
		R_1	R_2	R_3	C_1	C_2	C_3
550	9.381	12.33	118.7	219	0.658	0.9818	4.649
495	21.87	35.09	444.8	1246	0.5409	0.8678	3.787
440	58.66	52.85	884.5	1.219×10^4	0.3709	0.7384	1.263
385	165.7	99.17	1476	3.507×10^4	0.0651	0.3469	0.5994

Table 3. *ECM results of Pt electrode in 8% O_2.*

T (°C)	R_s (Ω m^2)	R_n(Ω m^2)			C_w(×10^{-4}F cm^{-2})		
		R_1	R_2	R_3	C_1	C_2	C_3
550	9.699	21.56	270.3	676.3	0.607	0.8748	5.21
495	23.41	49.24	847.8	6902	0.1105	0.2519	0.6493
440	57.39	151.3	2629	4.572×10^4	0.1426	0.1997	0.4056
385	175.4	104.4	5199	1.014×10^5	0.042	0.1175	0.223

Table 4. *ECM results of Pt-BaO electrode in 800ppm NO and 8% O_2.*

T (°C)	R_s (Ω m^2)	R_n(Ω m^2)			C_w(×10^{-4}F cm^{-2})		
		R_1	R_2	R_3	C_1	C_2	C_3
550	12	13.78	105.5	381	0.7519	1.875	6.72
495	28.95	30.31	272.7	1108	0.5027	1.127	3.873
440	82.78	56.72	587.5	2968	0.2465	0.708	2.417
385	239.7	94.8	835.2	6924	0.0029	0.398	1.224

Table 5. *ECM results of Pt-BaO electrode in 800ppm NO.*

T (°C)	R_s (Ω m^2)	R_n(Ω m^2)			C_w(×10^{-4}F cm^{-2})		
		R_1	R_2	R_3	C_1	C_2	C_3
550	11.66	12.98	93.21	208.3	1.326	2.241	3.522
495	28.52	30.84	251.6	1049	0.802	2.022	6.891
440	81.57	64.43	560.3	3291	0.464	1.215	3.436
385	232.5	91.53	776.8	7207	0.0028	0.4399	1.299

Table 6. *ECM results of Pt-BaO electrode in 8% O_2.*

T (°C)	R_s (Ω m^2)	R_n(Ω m^2)			C_w(×10^{-4}F cm^{-2})		
		R_1	R_2	R_3	C_1	C_2	C_3
550	11.87	14.31	120.1	507.3	0.8713	2.101	6.811
495	29.01	31.11	317.6	1652	0.5392	1.255	3.781
440	81.98	59.69	670.9	4785	0.2579	0.7463	2.078
385	233.2	96.86	950.4	1.061×10^4	0.0035	0.3323	0.93

As was shown in Tables 7 and 8, the summit frequencies at different temperatures were given. The arc 1 relative to the high frequency process ranged from 10 Hz to 1×10^4 Hz. The middle frequencies were from 1Hz to 10 Hz and low frequencies varied from 0.01Hz to 1Hz. The activation energy values in Pt-BaO electrode were lower than the Pt electrode in three arcs. Arc 1 showed the lowest activation energy and arc 3 showed the largest.

Table 7. *The summit frequencies of the fitted arcs in EIS results in 800ppm NO with 8% O_2 on Pt electrode.*

Arcs in EIS	Frequency Hz)	f_m (Hz)				E(eV)
		Pt				
		550°C	495°C	440°C	385°C	
1(high)	$10\sim10^4$	127.24	107.6	117.27	285.72	0.574
2(middle)	1~10	5.77	3.79	2.86	2.45	0.941
3(low)	0.01~1	0.39	0.26	0.09	0.08	1.273

Table 8. *The summit frequencies of the fitted arcs in EIS results in 800ppm NO with 8% O_2 on Pt-BaO electrode.*

Arcs in EIS	Frequency (Hz)	f_m (Hz)				E(eV)
		Pt				
		550°C	495°C	440°C	385°C	
1(high)	$10\sim10^4$	153.7	104.5	113.9	5776	0.54
2(middle)	1~10	8.05	5.18	3.83	4.79	0.583
3(low)	0.01~1	0.62	0.37	0.22	0.19	0.817

As can be shown in figure 12 to figure 14, the dependence of temperature on the serial resistances and polarization resistances were plotted in 800ppm NO with 8% O_2 on two cells. Results showed that the activation energy of the serial resistance Rs which was relative to the conductivity of the electrolyte for the two electrodes were close to each other. The activation energy in each arcs were calculated according to the equation (4). The activation energy of the total polarization resistance Rp for the Pt-Ba electrode and Pt electrode were 0.776eV and 1.238eV respectively in 800ppm NO with 8% O_2. The results were very close to the results obtained in the pure 8% O_2 atmosphere. And the activation energy were 0.817eV and 1.333eV for the Pt-BaO electrode and Pt electrode. This results were very close to the O_2 reduction reaction activation energy on Pt electrode studied by Bauerle [31]. And the value was between 1.43eV and 1.78eV. The results demonstrated that the adsorption decomposition of O_2 can be the controlling reaction step.

The activation energy appeared in arc 3 in the low frequency (0.01Hz-1Hz) for the Pt-BaO electrode and Pt electrode were 0.817eV and 1.273eV respectively in NO with O_2 atmosphere. While in 800ppm NO, the values were 0.987eV and 1.473eV and the values in 8% O_2 were 0.858eV and 1.413eV respectively indicating the NO or O_2 related reaction processes were included in this region. The activation energy in NO with O_2 appeared the lowest. The activation energy values in this frequency range were close to the results shown by Hansen [25, 29, 32]. As can be obtained from the results, the Pt-BaO electrode showed lower activation energy than the Pt electrode. The resistances varied less with the temperature in the Pt-BaO electrode. This may be controlled by the diffusion process of the reactants in the electrode. Therefore, the processes appeared in arc 3 may be related with the adsorption, surface diffusion, transfer of O_2 and NOx intermediates near/at the triple phase boundary (TPB). and the dissociative adsorption of O_2.

The activation energy for the Pt-Ba electrode and Pt electrode in the high frequency (arc 1, 10Hz-10^4Hz) were 0.54eV and 0.574eV respectively in NO with O_2. The values were close to each other in three different atmospheres on two cells. The reaction processes in high frequency arc were related to the diffusion of oxide ions to the electrode/electrolyte interface and charge transfer of oxide ions from electrode/electrolyte interface to the electrolyte [29, 33]. The activation energy in the middle frequency (arc 2, 1Hz~10Hz) may be attributed to the charge transfer reactions in the electrode and the adsorption decomposition of O_2 cause the activation energy were between the high and low frequency range. The activation energy were 0.583eV and 0.941eV for the Pt-BaO electrode and Pt electrode in NO with O_2.

Results showed that the decrease of activation energy in the middle and low frequency range became more significant in the Pt-BaO electrode. The improvement of the reaction performance may have relations with the processes of NO oxidation to NO_2, NOx storage in the form of Ba $(NO_3)_2$, and the Ba $(NO_3)_2$ decomposition to N_2 with external electrical field. The analysis of the experiments was consistent with the polarization results in I-V curves and CV tests. Thus, the proposed mechanism in Pt-BaO electrode can be described in figure 15: NO can be oxidized to NO_2 on the Pt surface. And NO and NO_2 can be stored in the adsorption layer in the form of Ba $(NO_3)_2$. The decomposition of Ba $(NO_3)_2$ under polarization decreases the reaction path of NO electrochemical reduction.

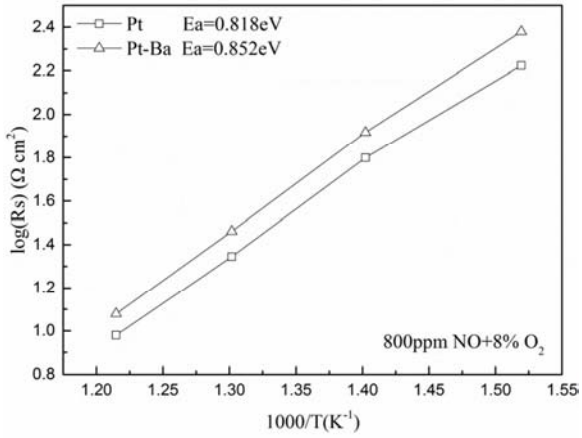

Figure 12. *Serial resistances(Rs) for the Pt-BaO electrode and Pt electrode in 800ppm NO with 8%.*

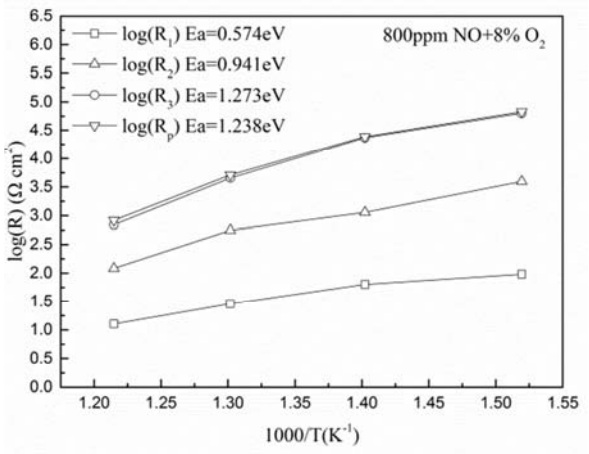

Figure 13. *Polarization resistances(R_p) for the Pt electrode in 800ppm NO with 8% O_2.*

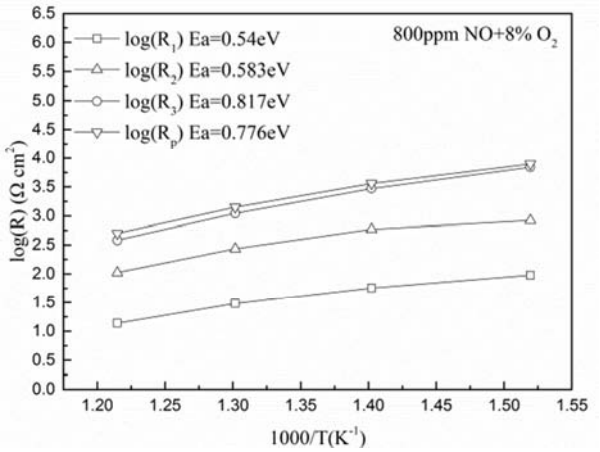

Figure 14. *Polarization resistances(R_p) for the Pt-BaO electrode in 800ppm NO with 8% O_2.*

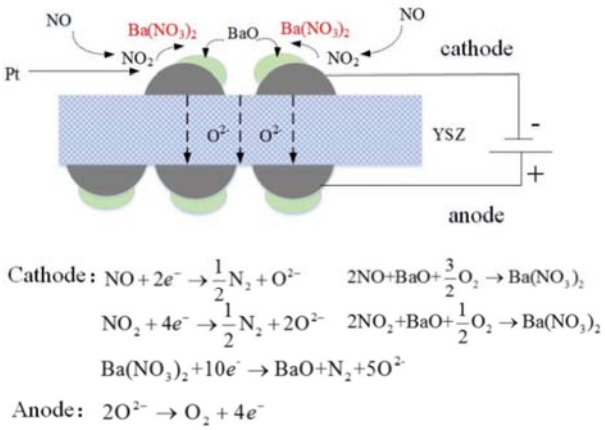

Figure 15. *The proposed improved reaction mechanism of NO electrochemical reduction in Pt-BaO electrode.*

4. Conclusion

The NO electrochemical reduction performances on the Pt electrode and the Pt-BaO electrode were studied by linear sweep voltammetry and CV tests. Results showed that the Pt-BaO electrode showed better activity and selectivity than the Pt electrode in NO atmosphere according to the CV measurements and I-V polarization curves. The electrochemical performance of NO on Pt-BaO electrode was superior to that on Pt electrode.

Electrochemical impedance spectra results showed that the resistances obtained on Pt-BaO electrode were far smaller than the results in the Pt electrode. The resistances in the O_2 containing atmospheres were larger than the pure NO atmosphere in two cells at high temperatures. The resistance in the NO with O_2 atmosphere decreased more significantly with Ba adsorption layer which was mainly ascribed to the acceleration of the surface diffusion, adsorption decomposition of O_2 and transfer of the O_2/NO components near/at the TPB. The activation energy in Pt-BaO electrode were lower than the Pt electrode in three different atmospheres. The proposed mechanism may be concluded as: NO can be oxidized to NO_2 on the Pt surface. And NO and NO_2 can be stored in the adsorption layer in the form of Ba $(NO_3)_2$. The decomposition of Ba $(NO_3)_2$ under polarization decreases the reaction path of NO electrochemical reduction. Adding Ba adsorption layer can trap NO in the active sites and thus the NO removal performance can be strengthened.

References

[1] J. C. Summers, S. V. Houtte, D. Psaras. Simultaneous control of particulate and NO emissions from diesel engines [J]. Applied Catalysis B: Environment, 1996, 10: 139-156.

[2] M. T. Lerdau, J. W. Munger, J. D. Jacob, "The NO_2 flus conundrum [J]," Science, 2000, 289: 2291-2293.

[3] Z. M. He, K. B. Andersen, L. Keel, F. B. Nygaard, M. Menon, K. K. Hansen. Processing and characterization of porous electrochemical cells for flue gas purification [J]. Ionics, 2009, 15: 427-431.

[4] T. J. Huang, C. Y. Wu, S. H. Hsu, C. C. Wu. Complete emissions control for highly fuel-efficient automobiles via a simulated stack of electrochemical-catalytic cells [J]. Energy & Environmental Science, 2011, 4: 4061-4067.

[5] T. J. Huang, C. Y. Wu, C. C. Wu. Lean-burn NOx emission control via simulated stack of solid oxide fuel cells with Cu-added (LaSr)MnO_3 cathodes [J]. Chemical Engineering Journal, 2011, 172 (2-3): 665-670.

[6] M. Awano, Y. Fujishiro, K. Hamamoto. Advances in nano-structured electrochemical reactors for NOx treatment in the presence of oxygen [J]. International Journal of Applied Ceramic Technology, 2004, 1 (3): 277-286.

[7] K. K. Hansen. Solid state electrochemical DeNOx-An overview [J]. Applied Catalysis B: Environmental, 2010, 100 (3-4): 427-432.

[8] T. J. Huang, C. Y. Wu, D. Y. Chiang, C. C. Yu. Ambient temperature NOx emission control for lean-burn engines by electro-catalytic tubes [J]. Applied Catalysis A: General, 2012, 445-446: 153-158.

[9] T. J. Huang, C. L. Chou. Feasibility of simultaneous NO reduction and electricity generation in SOFCs with V_2O_5 or Cu added LSCF-GDC cathodes [J]. Electrochemistry Communications, 2009, 11 (2): 477-480.

[10] R. M. L. Werchmeister, K. K. Hansen. Electrochemical reduction of oxygen and nitric oxide at low temperature on $Ce_{1-x}Pr_xO_{2-\delta}$ cathodes [J]. Electrochimica Acta, 2013, 114: 474-477.

[11] T. J. Huang, C. Y. Wu, Y. H. Lin. Electrochemical enhancement of nitric oxide removal from simulated lean-burn engine exhaust via solid oxide fuel cells [J]. Environmental Science & Technology, 2011, 45: 5683-5688.

[12] K. K. Hansen, E. M. Skou, H. Christensen. Perovskites as cathodes for nitric oxide reduction [J]. Journal of The Electrochemical Society, 2000, 147 (5): 2007-2012.

[13] C. G. Schmidt, D. Ippolito, J. J. Bentzen, K. B. Andersen, A. Kaiser, K. K Hansen. Fabrication and characterization of multi-layer ceramics for electrochemical flue gas purification [J]. Journal of The Electrochemical Society, 2013, 160 (9): E113-E119.

[14] A. de Lucas-Consuegra, A. Caravaca, M. J. Martín de Vidales, F. Dorado, S. Balomenou, D. Tsiplakides, P. Vernoux, J. L. Valverde. An electrochemically assisted NOxstorage/reduction catalyst operating under fixed lean burn conditions [J]. Catalysis Communications, 2009, 11 (4), 247-251.

[15] J. Shao, K. K. Hansen. Optimization of an electrochemical cell with an adsorption layer for NOx removal [J]. Journal of Solid State Electrochemistry, 2012, 16 (10): 3331-3340.

[16] R. M. L. Werchmeister, K. K. Hansen, M. Mogensen. Electrochemical removal of NOx with porous cell stacks[J]. Materials Research Bulletin, 2010, 45: 1554-1561.

[17] S. Bredikhin, K. Maeda, M. Awano. Electrochemical cell with two layers cathode for NO decomposition [J]. Ionics, 2001, 7 (1-2): 109-115.

[18] S. Bredikhin, K. Maeda, M. Awano. NO decomposition by an electrochemical cell with mixed oxide working electrode [J]. Solid State Ionics, 2001, 144 (1-2): 1-9.

[19] S. Bredikhin, K. Maeda, M. Awano. Low current density electrochemical cell for NO decomposition [J]. Solid State Ionics, 2002, 152-153: 727-733.

[20] K. Hamamoto, Y. Fujishiro, M. Awano. Low-temperature NOx decomposition using an electrochemical reactor [J]. Journal of The Electrochemical Society, 2008, 155 (8): E109-E111.

[21] X. Li, P. Vernoux. A new NOx storage-reduction electrochemical catalyst [J]. Applied Catalysis B: Environmental, 2005, 61 (3-4): 267-273.

[22] W. Y. Hernandez, A. Hadjar, A. Giroir-Fendler, P. Andy, A. Princivalle, M. Klotz, A. Marouf, C. Guizard, C. Tardivat, C. Viazzi, P. Vernoux. Electrochemically-assisted NOx storage-reduction catalysts [J]. Catalysis Today, 2015, 241: 143-150.

[23] C. G. Vayenas, S. Bebelis, S. Ladas. Dependence of catalytic rates on catalyst work function [J]. Nature, 1990, 343: 625-627.

[24] A. A. Nikola. NEMCA-From discovery to technology [J]. Catalysis Today, 2009, 146: 308-311.

[25] M. L. Traulsen, K. K. Hansen. Improvement of LSM15-CGO10 electrodes for electrochemical removal of NOx by KNO_3 and MnO_x impregnation [J]. Journal of The Electrochemical Society, 2011, 158 (12): P147-P161.

[26] M. L. Traulsen, F. Bræstrup, K. K. Hansen. NOx conversion on porous LSF15-CGO10 cell stacks with KNO_3 or K_2O impregnation [J]. Journal of Solid State Electrochemistry, 2012, 16: 2651-2660.

[27] M. L. Traulsen, K. B. Andersen, K. K. Hansen. NOx conversion on LSM15-CGO10 cell stacks with BaO impregnation [J]. Journal of Materials Chemistry, 2012, 22: 11792-11800.

[28] J. Shao, K. K, Hansen. Electrochemical NOx reduction on an LSM/CGO symmetric cell modified by NOx adsorbents [J]. Journal of Materials Chemistry A, 2013, 1: 7137-7146.

[29] J. Shao, K. K, Hansen. Enhancement of NOx removal performance for $(La_{0.85}Sr_{0.15})_{0.99}MnO_3/Ce_{0.9}Gd_{0.1}O_{1.95}$ electrochemical cells by NOx storage/reduction adsorption layers [J]. Electrochimica Acta, 2013, 90: 482-491.

[30] J. Shao. NOx reduction using an electrochemical cell with NOx adsorbents [D]. Denmark: Technical University of Denmark, 2013.

[31] J. E. Bauerle. Study of solid electrolyte polarization by a complex admittance method [J]. Journal of Physics and Chemistry of Solids, 1969, 30 (12): 2657-2670.

[32] R. M. L. Werchmeister, K. K. Hansen, M. Mogensen. Chracterization of $(La_{1-x}Sr_x)_sMnO_3$ and doped ceria composite electrodes in NOx-containing atmosphere with impedance spectroscopy [J]. Journal of The Electrochemical Society, 2010, 157 (5): P35-P42.

[33] M. J. Jorgensen, M. Mogensen. Impedance of solid oxide fuel cell LSM/YSZ composite cathodes [J]. Journal of The Electrochemical Society, 2001, 148 (5): A433-A442.